AIAA JOURNAL
Vol. 36, No. 5, May 1998

Viscous and Inviscid Vortex Generation During Startup of Rocket Nozzles

F. Nasuti* and M. Onofri†
University of Rome "La Sapienza," Rome 00184, Italy

An advanced numerical technique, based on the fitting and tracking of shocks, has been implemented to the simulation of flow transients during startup of axisymmetric rocket nozzles. The results show the occurrence of very peculiar flowfield configurations, not clearly in evidence in the current literature. In particular, two main vortical regions of different nature take place: The first has viscous origin, whereas the second is generated by typically inviscid phenomena. The evolution of these vortices and the interaction with each other and, possibly, with shocks plays an important role in the generation of pressure fluctuations on the nozzle wall and may yield nozzle side loads.

Introduction

DURING flow transients of rocket nozzles, as for example in the startup phase, the structure of the flowfield can be very different from the typical steady configuration. The flow evolution generally has a three-dimensional character with significant separated zones and intense shocks moving along the divergent section. Moreover, during the interval of time necessary to reach the final operating conditions in the chamber, the flow is highly unstable and is characterized by asymmetric zones of separated flow, which change their extent in time and move circumferentially around the nozzle wall.[1]

Knowledge of the origin of these phenomena, as well as the capability of predicting them, provides a challenging and intriguing academic motivation but also plays an important role in the design of nozzles of aerospace engines. Indeed, the phenomena may yield intense asymmetric forces on the nozzle wall during the engine startup or shutdown phases, possibly causing structural problems. The accurate prediction of such flowfields is, thus, mandatory but, despite the relevant applicative consequences involved, the origin of these side loads is not yet well understood.

Studies have been reported in the literature starting with pioneering analyses performed in the 1970s. In particular, the description of rocket nozzle startup transients was reported in Ref. 1. Wall pressure measurements, taken in that portion of the nozzle affected by the separated flow, show behavior characterized by fluctuations around an average value and sudden peaks, much higher than the average pressure value. That study[1] indicated flow separation as responsible for both wall pressure fluctuations and side loads, and it had an influence on the development of the few existing design methods, which assumed that hypothesis. Nevertheless, neither detailed experimental evidence nor any convincing explanation of the origin of the nozzle flow instability was provided.

From a numerical point of view some activities were undertaken to simulate nozzle flow transients, but not many studies have been carried out so far. Moreover, because the three-dimensional simulation requires an impractical amount of computational time, only two-dimensional plane or axisymmetric analyses have been performed. In Ref. 2 the transient of the Space Shuttle solid rocket booster (SRB) startup was studied by using the VNAP2 code, based on the McCormack scheme, whereas in Ref. 3 a time-accurate, pressure-based, reactive solver was used. In Ref. 4 calculations of the impulsive startup of an inviscid nonreacting gas through a shock tunnel nozzle by using the PARC code were presented. Better accuracy in the definition of flow discontinuities and more details on the flow structures were provided for viscous startup in Ref. 5, where the Unified Solution Algorithm code, a finite volume multizonal total variation diminishing (TVD) code, was used, and in Refs. 6 and 7, by a shock-fitting technique. The results of some of these studies[4,5,7] clearly indicated that the flowfield is characterized not only by the flow separation at wall, but also by the possible formation of a recirculating zone in the core flow of the divergent section. Unfortunately the latter phenomenon was not deeply discussed.

As a result of the foregoing survey, better knowledge of the basic physical phenomena seems to be necessary, as well as improvements in the techniques used for the numerical simulation. Aimed at filling this lack of knowledge, many studies have been carried out recently.[8] In this framework, the present study provides new insights in the description of the flowfield and in the possible explanation of the relevant phenomena. In particular, a numerical simulation has been performed mainly devoted to understand the origin and evolution of the two vortical structures generated during a nozzle startup transient: the first created by the viscous separation at the wall, the second by an inviscid production of vorticity behind the recompression shock that takes place in the divergent section. Because these vortical structures display a prominent effect on the wall pressure fluctuations, analyses have been carried out to describe their mutual interaction and to evaluate their role on the nozzle flow instability.

Numerical Simulation

The results of all of the numerical solutions performed so far indicate that the simulations of nozzle flow transients require high accuracy in handling shocks. This represents a problem from a numerical point of view. Indeed, a suitable number of mesh points should be used about the discontinuities, which unfortunately move all over the internal flowfield, usually in a way difficult to predict a priori. To avoid the use of computational grids with a great number of mesh points, an alternative way is to use adaptive grids changing in time, which, of course, burden the integration algorithm and involve long computational times.

A possible different approach, which has been used for the calculations presented here, is to treat the discontinuities by a fitting technique.[9] Accordingly, the shock points are explicitly fitted and tracked by a procedure that is an extension of the methodology proposed by Moretti[10] for inviscid flows. It provides a precise prediction of the location and propagation velocity of discontinuities. The solution technique is based on the nonconservative form of the Navier–Stokes equations, which are integrated by a second-order time- and space-accurate scheme that follows Moretti's lambda formulation for the convective terms[10] and uses central differencing for the viscous terms.[11] Compared with Ref. 10 and Ref. 11, this improved version displays a more robust character and better capability for handling general cases of interactions among discontinuities. The

Presented as Paper 96-0076 at the AIAA 34th Aerospace Sciences Meeting, Reno, NV, Jan. 15–18, 1996; received Jan. 14, 1997; revision received Sept. 22, 1997; accepted for publication Jan. 20, 1998.

*Ph.D., Postdoctoral Fellow, Dipartimento di Meccanica e Aeronautica, Via Eudossiana, 18. Member AIAA.

†Professor, Dipartimento di Meccanica e Aeronautica, Via Eudossiana, 18. Senior Member AIAA.

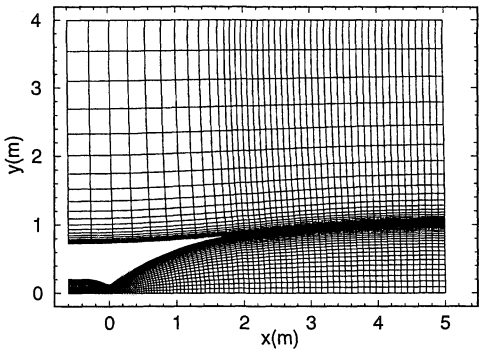

Fig. 1 Computational grid used for the viscous simulations.

results of many validation tests, including both plane and axisymmetric, viscous and inviscid flow transients, and exhaustive details are reported in Ref. 9.

In the present study the technique has been implemented to simulate the flow transient during startup of the HM60 nozzle of the Ariane 5 Vulcain engine. Both inviscid and viscous laminar flow models of a perfect gas, having $\gamma = 1.17$ and $R = 624$ J kg^{-1} K^{-1}, have been considered. In the viscous simulation, a linear dependence on temperature is assumed for viscosity μ and thermal conductivity k, $\mu/\mu_r = T/T_r$ and $k = \mu c_p/Pr$, using the reference air values $\mu_r = 1.786 \times 10^{-5}$ kg m^{-1} s^{-1}, $T_r = 300$ K, and $Pr = 0.72$. Quiescent gas at the ambient temperature and pressure ($T_a = 300$ K and $p_a = 1$ bar) in the nozzle is assumed as the initial condition. Varying inflow boundary conditions are imposed during the computation: total pressure and temperature increase from their ambient values to the chamber design values $T^0_{c,f} = 3527.1$ K and $p^0_{c,f} = 100$ bar. An adiabatic boundary condition on the wall and nonreflecting far field are assumed.

Typically, the flow features a three-dimensional character, and the transient in the chamber is at least 1 s long, with pressure and temperature growths following laws different from each other. Nevertheless, to have affordable computational times, the numerical simulations performed consider shorter transients of axisymmetric flows. These hypotheses, although not well suited for a detailed prediction of the flow transient, allow the analysis and a qualitative interpretation of the origin of some basic phenomena that, indeed, have been shown to scale with the transient length.[12]

In particular, a linear transient of 100 ms (LT100) has been considered as reference solution. It is characterized by a linear growth of total pressure and temperature, reaching the chamber operating values from the ambient conditions in $\Delta t_0 = 100$ ms.

The computational grid considered is orthogonal (Fig. 1). It includes 1) a lower region covering the nozzle inner field, which is 2.6 m long (90 × 40 nodes); 2) an external region from the nozzle exit section to the far-field outflow, which spans 5 m away from the nozzle throat (30 × 40 nodes from the nozzle exit); and 3) an upper external region, which has a total height of 4.0 m from the axis (46 × 30 nodes). The grid is stretched in the direction normal to the wall to cluster the mesh nodes inside the boundary layer. Comparisons with the results obtained by finer grids have shown that the minimum mesh size must be smaller than $(\Delta y)_i = 90$ μm at the inflow section.

Analysis of Nozzle Startup

The main features of the computed flowfield can be clearly analyzed by Fig. 2 (flow is from left to right), in which a flow visualization of the first 40 ms of the transient is provided by a sequence of instantaneous streamline patterns and fitted shock points, indicated by bold dots.

As pressure starts rising in the chamber, an incident shock with higher pressure on its left side appears in the nozzle and propagates quickly downstream. At the shock passage, a flow that follows the shock is generated from the nozzle entrance.

When the shock enters the divergent duct, a strong expansion occurs in the flow following the shock, and the flow behaves like in an overexpanded regime. To raise the pressure from the low values of the throat region to the higher values of the region following the incident shock, a compression takes place. As a consequence, the flow displays an adverse pressure gradient along the wall of the divergent section, which yields the two main features of these transients: the separation of the viscous boundary layer from the wall and the formation of a recompression shock in the supersonic core flow, located in correspondence with the maximum thickness of the separated region.

Flow Separation

The typical evolution in time of the flow separation is shown by Fig. 2. In particular, Figs. 2a and 2b show the onset of the separation, whereas Figs. 2b and 2c show the flow structure when the separated region is well formed, characterized by an intense vortex that takes place in correspondence of a pressure minimum.

After the formation of the separated flow region, the viscous nature of the flow leads to further separations downstream of the first separation point and to the generation of smaller vortices within that region (Figs. 2e–2g). Therefore, the separated region is characterized by two kinds of vortical structures: a main large vortex, with the axis located at the right boundary of the recirculating region, and smaller vortices, generated between the main vortex and the separation point.

As time elapses, the separated region extends, preserving its flow structure qualitatively similar in time. The evolution in time of this region can be described by the behaviors of its two ends: the separation point and the axis of the main vortex. On one hand, as the pressure grows in the chamber, the location where overexpanded conditions occur moves downstream along the divergent section. Accordingly, both the separation point and the recompression shock move slowly toward the nozzle exit. On the other hand, the movement of the main vortex is driven by the movement of the pressure minimum, which propagates downstream faster ($\simeq$240 m/s) than the separation point. In a few milliseconds, the separated zone is so stretched that it covers all of the region near the wall of the divergent section, from the separation point to the nozzle exit.

Inviscid Vortex Generation

While the separated region is enlarging, the main exhaust flow and the recompression shock evolve in a very peculiar jet about the nozzle centerline, bounded by the vortical separated region. Indeed, because the flow expansion behind the throat is not uniform in the radial direction, the intensity of the recompression increases, going from axis to wall. Different shock intensities along the shock profile are practically achieved in unsteady conditions by different shock propagation velocities. As a consequence, in this early phase during which the expansion is stronger at the wall than along the axis, the upper part of the recompression shock needs to experience a more intense pressure jump and thus moves downstream slower than the lower part. The shock shape is thus bent upstream, with the lower part almost normal to the axis.

After a few milliseconds the recompression shock changes its profile, and displays a Y shape, characterized by a shock interaction in a triple point, which separates the downstream flowfield into two zones: the upper zone where a supersonic jet takes place through the two oblique shocks and the lower zone with a normal shock and a recirculating subsonic region behind it.

Important practical consequences come from the generation of this second vortical region. Because it displays origins and nature very different than the vortical separated region at wall and strongly depends on the evolution of the recompression shock, an analysis of the formation of the Y shape of this shock is provided in the following.

A few instants after its onset (Fig. 2a), the shock is completely formed across the divergent section (Fig. 2b). Afterwards, the interaction between the bubble of separated flow at the wall and the main exhaust jet leads to a turning of the supersonic stream pattern and to the formation of an oblique shock branch from the separation point, which interacts with the recompression shock. Behind this shock branch, the pressure value upstream of the recompression shock is higher than at the axis; therefore, the needed pressure recovery that occurs across this side of the recompression shock and the consequent shock intensity are lower.

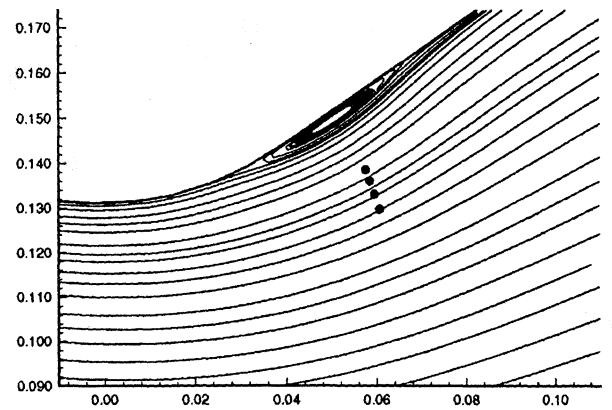

a) t = 2 ms

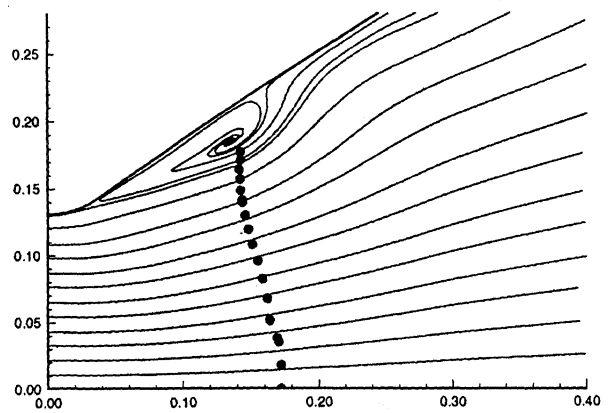

b) t = 2.5 ms

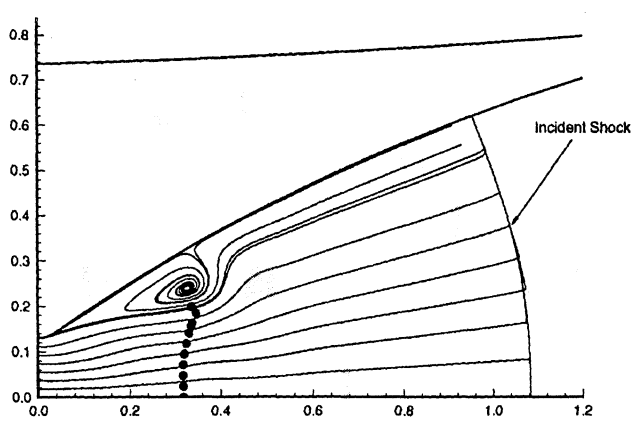

c) t = 3.25 ms

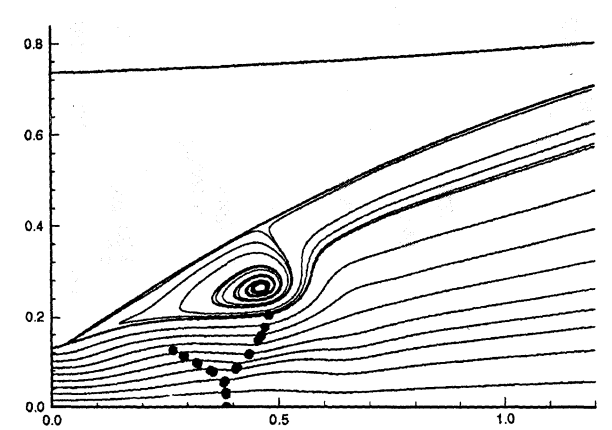

d) t = 3.75 ms

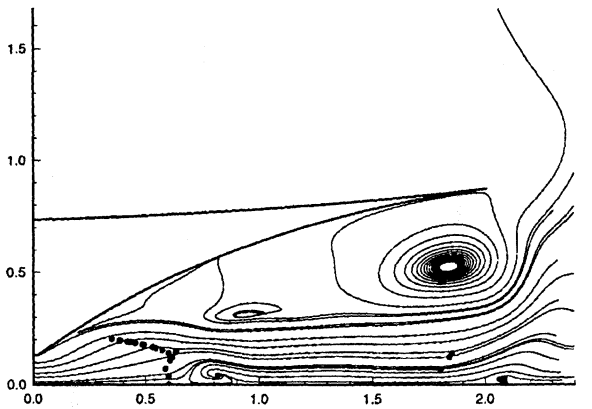

e) t = 10 ms

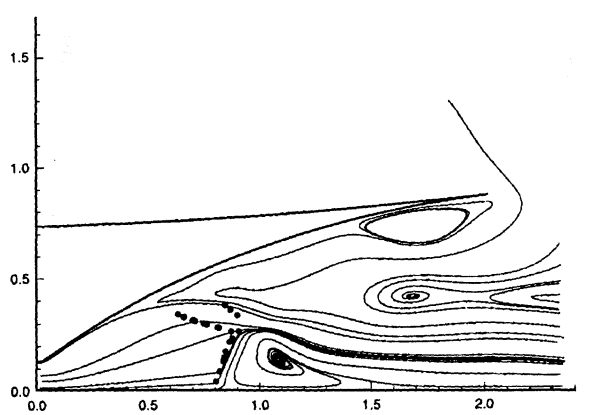

f) t = 17.5 ms

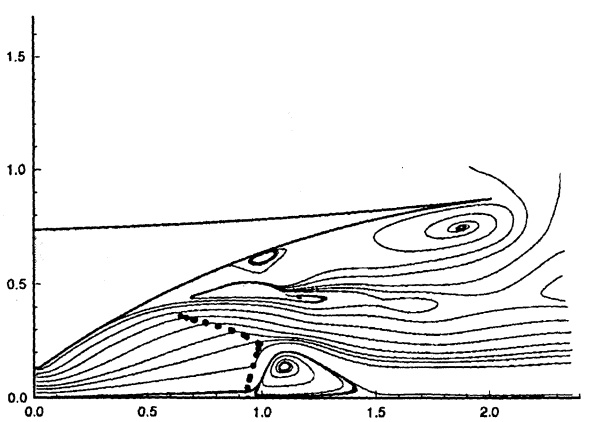

g) t = 25 ms

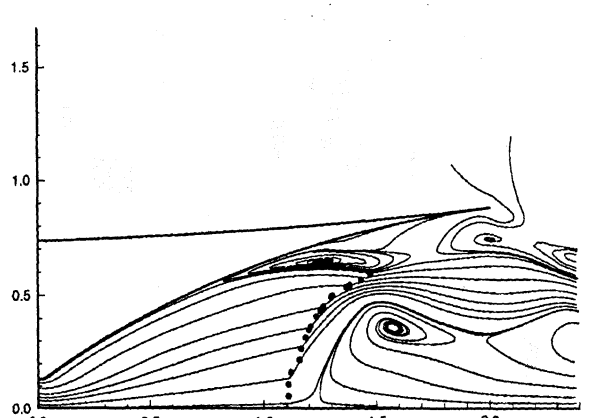

h) t = 40 ms

Fig. 2 Instantaneous streamlines and shock points (•) for the viscous simulation of LT100.

As a result, the upper part of the recompression shock moves faster than the lower part and the shock is thus bent downstream, with the lower part almost normal to the axis. The resulting shock shape, therefore, features the typical flow structure that characterizes the flow transient in the divergent section: a separated region at the wall and a Y-shaped recompression shock (Fig. 2d), with supersonic flow in the upper zone and subsonic in the lower.

The different strength and shape of the shock from the axis to the separation line cause high velocity and entropy gradients behind the shock itself. This yields high vorticity in the region. In fact, at $t = 10$ ms (Fig. 2e) a vortex already took place behind the normal branch of the Y shock, in the region close to the axis.

It is also worthwhile to note that further variations of the shock intensity are caused by the nonuniform flow in the radial direction, due to both the geometry of the divergent section and the increasing pressure and temperature in the chamber. The final result is a shock stronger at the axis than at the wall.

In the following times, the vortex enlarges in such a way that it spreads over a large part of the divergent section. Moreover, as the recirculating zone enlarges, other smaller vortices are created about the main one.

Therefore, another vortical region, having a different origin than the viscous separated region, appears behind the recompression shock, about the axis. It can be called inviscid vortical zone, in accordance with its nature, which appears, indeed, similar to that of the vortical phenomenon specifically discussed in a workshop whose results were reported by Salas.[13] The existence of Euler solutions was indicated that feature recirculating flow bubbles behind the shock that occurs in transonic flows over a circular cylinder and thus was denoted as inviscid separation. Reference 13 and other later studies[14,15] indicated that the viscous effects may have a marginal role in the evolution of these recirculating regions for high Reynolds number flows. Following this interpretations, computations of high-speed flows showing vortices generated by inviscid entropy gradients have been successfully performed by solving Euler equations[16–18] and have been also used to explain the irregular behavior of experimental results.[17]

The recirculation bubble initially covers only a very small region of the flowfield compared with the very large region occupied by the viscous vortices of the separated flow region. Later on, as time elapses, the separation point moves toward the exit and the separated region shrinks, while the inviscid vortical region becomes larger and larger (Figs. 2g and 2h).

The occurrence of an inviscid vortex and of a reverse flow in the core of a nozzle divergent section have never been stressed in the literature. Only a few flowfield representations suggest that such structures were actually computed, even if not discussed.[4,5,7] On the contrary, the evolution of this vortex is of great importance for the understanding of the physical phenomena of the nozzle startup or shutdown and, particularly, for its practical consequences on the nozzle flow stability as shown in the following.

Although other numerical solutions, independently of the integration scheme and the test considered, also showed a similar flow structure, objections could be raised on the physical nature of the mechanism that generates the phenomenon, due to the possible role of the artificial dissipation.

Concerning this issue, it should be emphasized that the integration technique used in the present study displays features so as to minimize the influence of numerics on the results. In particular: 1) no explicit artificial damping to stabilize the solution was added, thereby taking full advantage of the shock-fitting technique adopted and 2) a global minimum integration time step was used to preserve the physical meaning of the time-dependent simulation; this feature also allows avoiding the consequences of the use of a local time step that could affect the structure of the recirculating flow region as indicated by Salas.[14] As a result of these choices, a numerical dissipation of the scheme can be produced only by the order of accuracy of the solution and, thus, eventually it depends on the grid mesh size adopted. We can, therefore, say that qualitatively the results are correct and that considerations made on that basis about the physical meaning of the phenomena analyzed are admissible.

Of course, the quantitative precision of the solution may be still questionable. Indeed, this is a well established and unsolved problem in every vortical flowfield, because the local quality of the solution depends on the grid mesh size adopted and, in particular, on the possibility that it can appreciate the smallest vortex scale that takes place in the flow. An example of these difficulties is provided by Ref. 19, where in recirculating flow regions a full grid convergence also is not achieved by using very fine grids. Nevertheless, this is a local effect that does not much affect the quality of the solution in the remaining part of the flowfield, where grid convergence is actually obtained.

In conclusion, the present study does not claim to provide a detailed prediction of the phenomenon, but only aims to use the qualitative indications of the results to give insight into its still unclear physical origin.

Pressure Loads on the Wall

From a practical point of view, a very important consequence of the described flow structure can be noted from Figs. 2e–2h within the divergent section. The exhaust jet flows in a narrow channel between the two vortical zones, circumventing the recirculating region behind the recompression shock and bounded in the upper zone by the separated flow region. As shown in Fig. 2, the exhaust flow thus undertakes sudden shrinking and expansions, which yield wave propagation phenomena in the radial direction, with consequent wall pressure loads.

The sequence of Figs. 3a–3c shows the typical effects of this wave propagation on the wall. At $t = 40.0$ ms, the recompression shock is close to the nozzle exit, the inviscid vortex covers a large part of the divergent section, the viscous separated region is shrunken to a

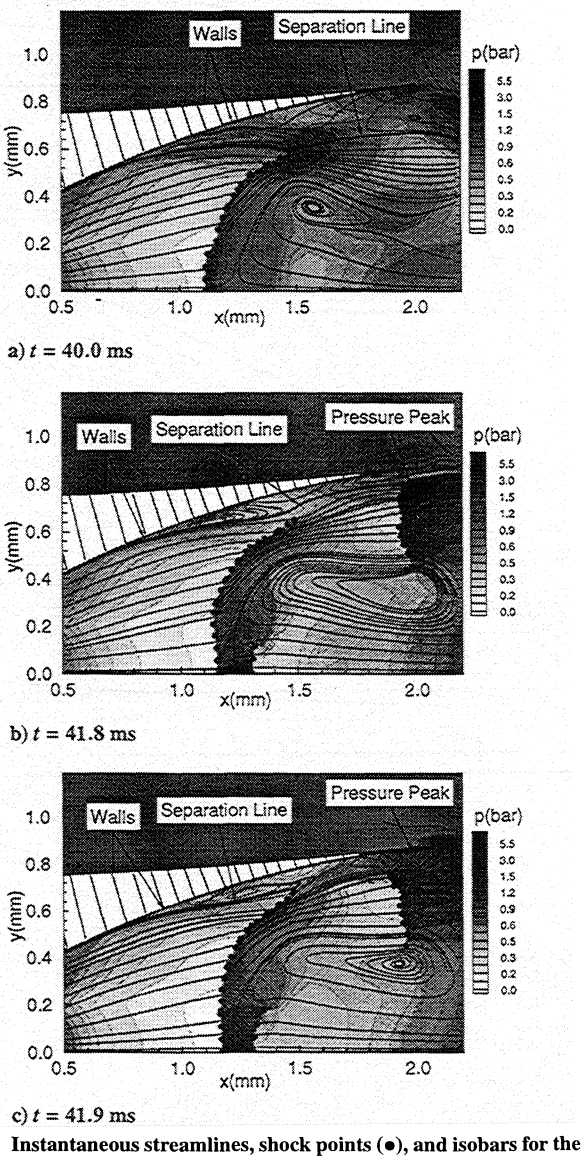

Fig. 3 Instantaneous streamlines, shock points (•), and isobars for the viscous simulation of LT100.

very limited zone about the nozzle edge, and the main exhaust jet flows in a narrow space, bounded by the two recirculating zones.

At $t = 41.8$ ms the space for the high-speed exhaust jet is so reduced that the flow is obstructed and a shock takes place, with a sudden rise of pressure behind it. As a consequence, a wave propagation is generated in the radial direction. In Fig. 3c, at $t = 41.9$ ms, its effect is clearly visible: the separated region is shrunken against the wall and the high pressure reaches the wall itself, yielding a jump in the local pressure value. Afterwards, it is reflected and propagates downstream.

This sequence confirms that the origin of high-pressure peaks on the wall is related to the obstruction that the viscous and especially the inviscid recirculating regions yield on the main exhaust jet and to the intense shocks, with the consequent sudden pressure rises, that they produce within the jet itself.

These considerations are limited to axisymmetric calculations, whereas it is well known that predictions of side loads would require three-dimensional simulations. Nevertheless, although three-dimensional calculations are always a hopeful evolution of the future studies on this topic, it is worthwhile to note that the present axisymmetric considerations have a more general value. Indeed, it is well known that an axisymmetric vortex in an internal flow, like the discussed inviscid vortex in the core flow, is a quite unstable structure. Depending on an even small circumferential nonuniformity, it is very likely that it degenerates toward an asymmetric configuration.

Wall Pressure Behavior

The origin of the rocket nozzle side loads during startup was commonly explained in the literature as a consequence of the viscous separation of the boundary layer from the wall. Nevertheless, the numerical results just described can provide a more articulated explanation. In particular, other phenomena, related to the transient character of startup flows and to the generation of a recirculating flow region in the nozzle core, could explain the origin of side loads, as the following analysis of wall pressure behavior would also suggest.

Figure 4 shows the time history of the wall pressure computed in five locations of the divergent section; the ambient pressure $p_a = 1$ bar has been assumed as reference pressure. The behaviors display fluctuations of different intensity and frequency. In the early time only fluctuations of low intensity take place, but later and in points closer to the nozzle exit the fluctuations have greater intensity, with the occurrence of isolated high peaks. As indicated in the following, these fluctuations are related to phenomena having a different nature, and only part of them can be associated to the occurrence of the viscous flow separation.

In particular, three different kinds of fluctuations occur.

1) Low-frequency fluctuations are detectable at $x = 0.4$ and 0.8 m, having amplitude of the order of magnitude of 0.3 bar and having two peaks at about 8 and 20 ms in both cases, as well as one at about 15 ms.

2) High-frequency fluctuations are detectable at $x = 0.4$ m as the small-amplitude ones (<0.1 bar) superimposed to fluctuations 1 between 10 and 30 ms.

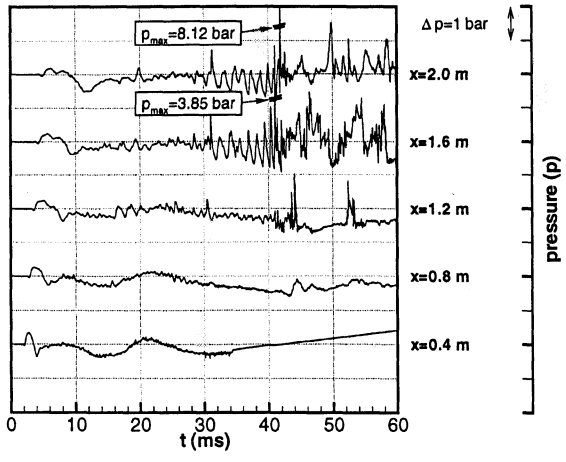

Fig. 4 Pressure time history at five locations on the divergent section wall for the viscous simulation of LT100 (x = distance from the throat).

3) High-frequency and amplitude fluctuations are detectable at $x = 1.6$ and 2.0 m, occurring after $t = 30$ ms (amplitude of the order of magnitude of 0.5 bar before degeneration to more than 1 bar).

In the first phase of the transient ($t = 0$–10 ms), the wall pressure behaviors are characterized by the propagation of the incident shock. In Fig. 4 the pressure rise is more evident after 3–4 ms in the curves relevant to the positions at $x = 0.4$ and 0.8 m from the throat, whereas it tends to decrease in points downstream, due to the enlargement of the propagation front.

After the shock passage, a first minimum in the wall pressure history appears, due to the expansion in the throat region. It follows the incident shock, but it travels at lower speeds and, thus, the high pressure zone following the shock tends to extend. In fact, in the interval of time 0–10 ms the behaviors display wall pressure values almost constant between the first rise and the first minimum, and this zone tends to extend, as shown by the comparison of the curve at $x = 0.4$ m with those relevant to other points downstream.

At subsequent times, the behavior at $x = 0.4$ and 0.8 m clearly show the low-frequency fluctuations 1 (Fig. 4) of wall pressure. The phenomenon seems to be related to the reflection of the incident shock wave at the nozzle exit. Indeed, this explanation is consistent with an approximate prediction based on assumptions of a wave propagation occurring in a low-speed flow with the ambient value of speed of sound ($a = 468$ m/s). The wave becomes less clear in the behaviors computed in the other wall points, because of the other perturbations.

Superimposed on fluctuations 1 (Fig. 4), very small oscillations with high frequency take place. They are denoted as fluctuations 2 (Fig. 4). It is interesting to note that they appear in of all the behaviors, always occurring after the first pressure minimum and, therefore, after the separation of the boundary layer from the wall. Indeed, fluctuations 2 are one of the effects of the formation of the vortical separated region. The slight increase of their amplitude moving from sampling points located about the throat to those located downstream seems to be related to the increasing thickness of the separated flow region. Indeed, both the maximum velocity of the recirculating flow and the frequency of its impact on wall pressure depend on it.

As time elapses, a completely different wall pressure behavior occurs: more intense oscillations with slight lower frequency appear in the second-half of the transient, after $t = 30$ ms. They are denoted as fluctuations 3 (Fig. 4). Because they are recorded only in the sampling points closest to the nozzle exit, they should originate from phenomena occurring in late phase of the transient. In fact, the temporal correlation between the diagrams of Fig. 4 and the time evolution of the flow structures (Fig. 2) indicates that fluctuations 3 appear only when the inviscid recirculating region behind the recompression shock is fully developed. In this situation, the exhaust flow moves around this vortical zone changing in size, and the interaction with it yields a sequence of shrinking and expansions of the jet. The consequent changes in pressure are larger than the previous ones, because they are caused by variations in high-speed flow. The pressure history in the core flow is then transmitted by radial wave propagations toward the wall, leading a similar wall pressure behavior. The characteristic scale of this phenomenon is, therefore, of the order of magnitude of the local radius of the divergent section and, in fact, the phenomenon features a lower frequency.

During this last phase, fluctuations 3 also display pressure peaks much higher than their average amplitude. Values as large as $\Delta p = 7$ bar have been recorded. As indicated in the preceding section, these peaks have the same origin as fluctuations 3 occurring before $t = 40$ ms and, therefore, can be seen as dramatic aspects of the same physical phenomenon.

Inviscid Simulations

For practical purposes, it is important to analyze the possible correlations between the evolution of the flow structures discussed and the flow parameters that characterize the phenomenon and, in particular, the dependence on the flow conditions in the combustion chamber. To perform such studies, long computational times are necessary to simulate accurately the boundary-layer zone, whereas the extension to three-dimensional calculation is impractical.

Nevertheless, due to its inviscid origin, the basic behavior of the inviscid vortical zone can be analyzed by means of an inviscid simulation of the nozzle flow transient. It should also be considered that in the viscous simulation the extent of the separated region is small when the recompression shock is close to the nozzle exit, i.e., when the wall pressure instability is higher. In that phase, the inviscid vortex covers a large part of the divergent section and the flowfield displays a structure very similar to that generated by an inviscid simulation.

To exploit less burdensome simulation models, an inviscid analysis has been performed. Moreover, a reduced combustion chamber transient has been considered because it has been shown[12] that a scaling effect exists for evolutions characterized by shorter transients, provided they are not too fast to yield supersonic flow in the convergent section. It is a piecewise linear transient of 25 ms (PLT25), formed by two linear parts: the first one coincides with the initial 5 ms of LT100, whereas the second, lasting from $t = 5$ to 25 ms, completes the transient with a linear rise of chamber pressure and temperature from the conditions reached at the end of the first part to the final conditions.

The sequence of the inviscid results of PLT25 are shown in Fig. 5. They have been obtained by using three different grids (Table 1), over the same domain as Fig. 1.

Table 1 Grids used for refinement

	Lower region		
Grid	Nozzle	External	Upper region
1 (coarse)	74 × 10	26 × 10	40 × 10
2 (medium)	147 × 20	53 × 20	80 × 20
3 (fine)	220 × 30	80 × 30	120 × 30

The sequence of Fig. 5 displays the generation of the inviscid vortical zone behind the recompression shock, with the formation of the main and small vortices. Then, the main vortex becomes larger, spanning the entire nozzle radius. Qualitatively similar to the viscous solution, in this case also the wall pressure fluctuations are enhanced when the enlargement of the recirculating bubble is such that only a narrow channel is left to the main exhaust jet, where the gas flow at very high speed yielding shocklets and sudden pressure rises when the flow passage is more obstructed (Fig. 6).

An important conclusion of this analysis is that the main effects of the vortical structure in these nozzle flow transients may be qualitatively described under the inviscid hypothesis. That allows a

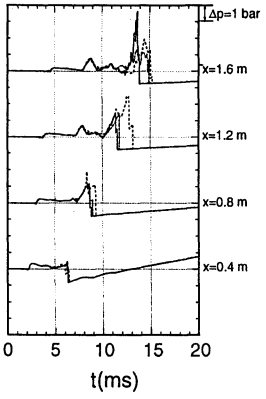

Fig. 6 Pressure time history at four positions on the divergent section wall for the inviscid simulation of PLT25 (x = distance from the throat): – – –, grid 1; –·–, grid 2; and ——, grid 3.

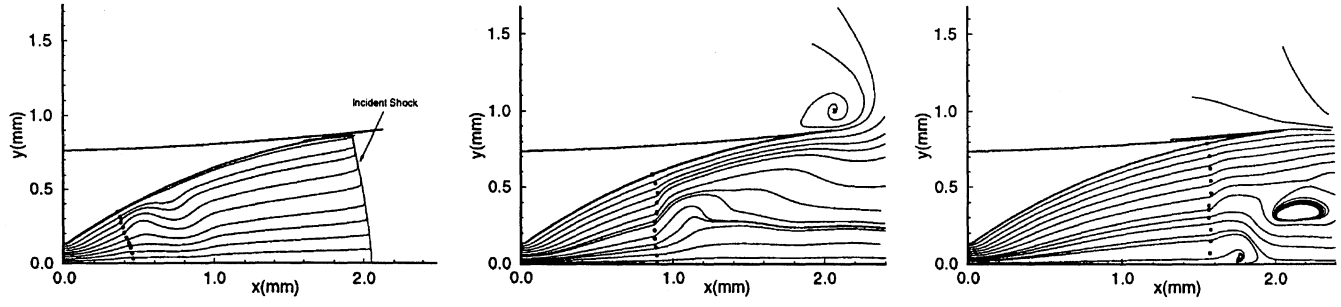

a) Grid 1, t = 5 ms d) Grid 1, t = 10 ms g) Grid 1, t = 15 ms

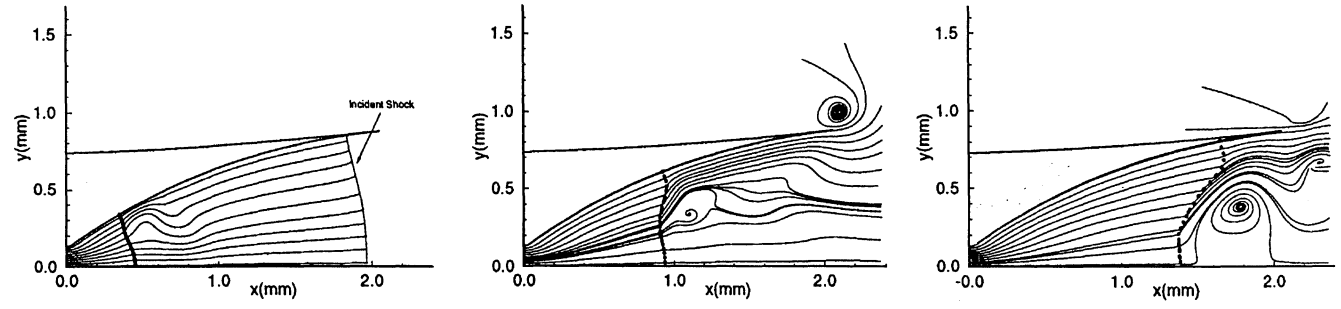

b) Grid 2, t = 5 ms e) Grid 2, t = 10 ms h) Grid 2, t = 15 ms

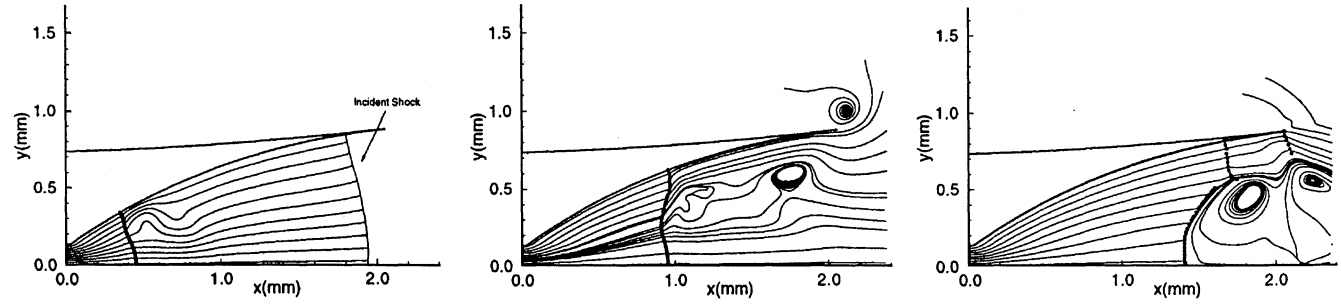

c) Grid 3, t = 5 ms f) Grid 3, t = 10 ms i) Grid 3, t = 15 ms

Fig. 5 Instantaneous streamlines and shock points (•) for the inviscid simulation of PLT25.

very significant saving of computational time, nonetheless preserving the main features of the flowfield.

The tests also provide an indication about the grid dependence of the numerical solution. Indeed, the results obtained with the three different grids emphasize the need of using sufficiently clustered computational meshes. In particular, the comparison among solutions is shown in Fig. 6: even if a full grid convergence cannot be achieved, the solutions display good agreement when the grid resolution allows a representation of the small vortices that take place behind the shock. A lack of resolution leads to displacements in the predictions of the extent of the bubble and of the location of the shock.

Conclusions

An advanced numerical technique based on shock fitting has been implemented to the simulation of axisymmetric flow transients of an aerospace engine nozzle. The results show the following.

1) During nozzle startup very peculiar flowfield configurations occur, which are characterized by two main vortical regions: the first is due to the boundary-layer separation from wall, whereas the second covers much of the divergent section and has an inviscid origin.

2) The inviscid vortices play an important role in the generation of wall pressure fluctuations and eventually of the nozzle side loads. This role was not clearly in evidence in the literature.

3) Inviscid calculations show the generation of a similar recirculation zone and, thus, they can represent a possible way to perform qualitative analyses of the phenomenon, by means of a less cumbersome approach than viscous solutions.

The continuation of the present work is in progress to evaluate the influence of different transients of the flow values in the combustion chamber on the evolution in time of the vortical regions.

Acknowledgments

The study was partially supported by Daimler–Benz Aerospace, in the framework of the ELITE Program of the European Space Agency on advanced nozzle technology. Partial support by Agenzia Spaziale Italiana is also acknowledged.

References

[1]Nave, L., and Coffey, G., "Sea Level Side Loads in High-Area-Ratio Rocket Engines," AIAA Paper, 73-1284, Nov. 1973.

[2]Cline, M. C., and Wilmoth, R. G., "Computation of the Shuttle Solid Booster Nozzle Start-up Transient Flow," *Journal of Propulsion and Power*, Vol. 1, No. 5, Sept. 1985, pp. 321–328.

[3]Wang, T.-S., "Numerical Study of the Transient Nozzle Flow Separation of Liquid Rocket Engines," *Computational Fluid Dynamics Journal*, Vol. 1, No. 3, 1992, pp. 319–328.

[4]McAmis, R. W., Lankford, D. W., and Phares, W. J., "Theoretical Liquid Rocket Engine Nozzle Flow Fields," AIAA Paper 92-3730, July 1992.

[5]Chen, C., Chakravarthy, S., and Hung, C., "Numerical Investigation of Separated Nozzle Flows," *AIAA Journal*, Vol. 32, No. 9, 1994, pp. 1836–1843.

[6]Onofri, M., and Nasuti, F., "Numerical Analysis of Nozzle Start-up," *Atti del XII Congresso Nazionale AIDAA*, Associazione Italiana di Aeronautica e Astronautica, Como, Italy, 1993, pp. 741–750.

[7]Nasuti, F., and Onofri, M., "Transient Flow Analysis of Nozzle Start-up by a Shock Fitting Technique," *Unsteady Flows in Aeropropulsion*, edited by W. Ng, D. Fant, and L. Povinelli, Vol. AD-40, ASME, New York, 1994, pp. 127–135.

[8]Caporicci, M., Eriksson, L., Pekkari, L., Onofri, M., Popp, M., and Weiland, C., "Advanced Nozzle Technologies for the Ariane 5 Vulcain Engine," AIAA Paper 94-3263, June 1994.

[9]Nasuti, F., and Onofri, M., "Analysis of Unsteady Supersonic Viscous Flows by a Shock Fitting Technique," *AIAA Journal*, Vol. 34, No. 7, 1996, pp. 1428–1434; also AIAA Paper 95-2159, June 1995.

[10]Moretti, G., "Efficient Calculations of 2D Compressible Flows," *Advances in Computer Methods for Partial Differential Equations*, Vol. 6, 1987, pp. 60–66.

[11]Moretti, G., Marconi, F., and Onofri, M., "Shock Boundary Layer Interactions Computed by a Shock Fitting Technique," *Lecture Notes in Physics*, Vol. 414, Springer–Verlag, New York, 1993, pp. 345–350.

[12]Nasuti, F., and Onofri, M., "Characteristic Scales of Unsteady Phenomena in Rocket Nozzles," *Computational Fluid Dynamics '96*, edited by J. Desideri, C. Hirsch, and P. L. Tallec, and M. Pandolfi, and J. Periaux, Wiley, Chichester, England, UK, 1996, pp. 711–717.

[13]Salas, M. D., "Recent Developments in Transonic Euler Flow over a Circular Cylinder," *Mathematics and Computers in Simulation*, Vol. 25, Elsevier Science, 1983, pp. 232–236.

[14]Kumar, A., and Salas, M. D., "Euler and Navier–Stokes Solutions for Supersonic Shear Flow past a Circular Cylinder," *AIAA Journal*, Vol. 23, No. 4, 1985, pp. 583–587.

[15]Buntine, J. D., and Pullin, D. I., "Merger and Cancellation of Strained Vortices," *Journal of Fluid Mechanics*, Vol. 205, Aug. 1989, pp. 263–295.

[16]Pandolfi, M., and Larocca, F., "Transonic Flow about a Circular Cylinder," *Computers and Fluids*, Vol. 17, No. 1, 1989, pp. 205–220.

[17]Botta, N., "The Inviscid Transonic Flow about a Cylinder," *Journal of Fluid Mechanics*, Vol. 301, Oct. 1995, pp. 225–250.

[18]Marconi, F., "On the Prediction of Highly Vortical Flows Using an Euler Equation Model," *Studies of Vortex Dominated Flows*, edited by M. Y. Hussaini and M. D. Salas, Springer–Verlag, New York, 1987, pp. 311–364.

[19]Weber, Y. S., Oran, E. S., Boris, J. P., and Anderson, J. D., "The Numerical Simulation of Shock Bifurcation Near the End Wall of a Shock Tube," *Physics of Fluids*, Vol. 7, No. 10, 1995, pp. 2475–2488.

K. Kailasanath
Associate Editor